



Article

Experimental and Numerical Investigations on Strains of Metal Sheet Parts Processed by Electromagnetic Forming

Dorin Luca ^{1,*} and Dorian D. Luca ²

¹ Faculty of Materials Science and Engineering, Technical University of Iasi, 700050 Iasi, Romania

² Young Independent Researcher, Engineer, 700360 Iasi, Romania; work.dorianluca@gmail.com

* Correspondence: dluca@tuiasi.ro

Abstract: Electromagnetic forming is applied to form metal sheet parts from both non-ferrous and ferrous materials. In this paper, the electromagnetic forming behavior of aluminum alloy, copper and steel sheets was investigated through experiments. The disk-shaped specimens were electromagnetically free bulged with increasing deformation energies and parts with different deformation depths were obtained. The deformation was done with and without clamping the movement of the specimens' edges. The specimens were printed with a mesh of diametrical lines and concentric circles with a predetermined pitch. The mesh served to determine the displacements in the mesh nodes after the deformation of the specimens, with which the axial, radial and circumferential strains were then calculated. The experimental data obtained was subjected to statistical correlation and regression analyses, and the mathematical models for the three main strains in each material were established. The strains of AlMn0.5Mg0.5 and Cu-OF parts are maximum in the center and have a similar variation, while the FeP04 parts have the maximum strains in an intermediate zone between the center and the edge.

Keywords: metal sheet; electromagnetic forming; strains; regression analysis; mathematical model



Citation: Luca, D.; Luca, D.D. Experimental and Numerical Investigations on Strains of Metal Sheet Parts Processed by Electromagnetic Forming. *J. Manuf. Mater. Process.* **2023**, *7*, 180. <https://doi.org/10.3390/jmmp7050180>

Academic Editor: Andrea Ghiotti

Received: 31 July 2023

Revised: 22 September 2023

Accepted: 3 October 2023

Published: 5 October 2023



Copyright: © 2023 by the authors. Licensee MDPI, Basel, Switzerland. This article is an open access article distributed under the terms and conditions of the Creative Commons Attribution (CC BY) license (<https://creativecommons.org/licenses/by/4.0/>).

1. Introduction

Electromagnetic forming (EMF) continues to be an attractive technique for plastic deformation and joining of different metallic materials. The working principle of the EMF process is based on the law of electromagnetic induction. Thus, the forming tool is a coil through which a high-intensity current flows, producing a variable magnetic field around it. This field induces in the workpiece a current in the opposite direction to that in the coil. The plastic deformation of the workpiece results from the repulsion action of the two currents of the opposite direction. The relevant characteristics of the EMF process consist in the possibility of significantly increasing the forming limits of metallic materials and significantly reducing the springback after deformation. Current researches are focused on evaluating the EMF capabilities of different metal sheets in order to manufacture parts with larger dimensions and surfaces that have certain curves. EMF is the only plastic deformation process in which the size of the obtained strains depends on both the mechanical properties of the material and its electrical conductivity.

Li et al. [1] studied the formability of low conductivity metal sheet (Ti-6Al-4V alloy) using EMF with a flat coil. The results show that the formability of the titanium alloy showed a significant increase compared to the formability under quasi-static deformation, with the highest percentage increase being close to 74% in the plane strain state. For the deformation of titanium alloys, known to have low conductivity and high strength, Feng et al. [2] propose a new method of EMF, called direct current pulse electromagnetic forming. The feasibility of the new method was demonstrated experimentally by forming a corrugated part of Ti-6Al-4V with high precision as a result of significant yield strength reduction by the heat that the Joule effect produced. The method has been successfully tested by

experiments to verify the forming of other hard-to-form materials at room temperature (aluminum alloy sheets) Feng et al. [3], taking a solid step towards achieving industrial application. A hybrid technique of forming a titanium sheet is used by Cai [4]. It uses forming with a flexible polyurethane tool actuated by vaporizing a film obtained through discharging a capacitor bank of an EMF installation. This technique's advantage is a better distribution of the deformation pressure on the workpiece surface. Dong et al. [5] address the EMF fabrication process of titanium bipolar plates for proton exchange membrane fuel cells. The authors established a coupled electromagnetic-mechanical 3D model to optimize the EMF process. The pressure actuator used ensured a uniform distribution of the deformation pressure, which allowed the obtaining of a titanium bipolar plate with the desired dimensions, low thinning (below 16%) and high corrosion resistance. Huang et al. [6] present another method for EMF processing of low-conductivity workpieces, such as stainless steel and titanium, where the electromagnetic force generated on the workpiece is low and not enough to deform the material. The drive forming method can be used for these materials, and the drive forming mechanism, effect of drive plate size, workpiece thickness and discharge frequency on the forming result have been studied through simulation and experiment.

Liu et al. [7] carried out a numerical and experimental study on the EMF of DP780 high strength steel sheets. The effects of strain rate on the DP780 mechanical properties were analyzed by quasi-static tensile test and Hopkinson bar test. The results showed that the yield strength and ultimate tensile strength of the material increased with the high strain rate, and the high strength steel DP780 shows some strain rate sensitivity. An EMF process of FeP04 steel sheets was studied in a wide range variation of technological parameters on the premise of finding the best values, which provide a maximum deformation of the part. The best predictions for the parameters taken into analysis were made by neural networks modeling [8].

Moreover, Jin and Yu [9] note an increase in the formability, but also the hardness at the same time, of 2195-T6 aluminum alloy sheet during EMF. The deformation behavior and corresponding hardening effect of a conical part were evaluated by strain analysis and Vickers hardness testing, respectively. Study demonstrates the room temperature EMF feasibility of ultra-high strength aluminum alloys. In the paper [10], Lin et al. studied the effect of EMF on the forming limit and properties of aluminum alloy 2024-O. Compared with quasi-static stamping, the forming limit of 2024-O alloy for EMF increased by close to 37%. For the same deformation height of over 17 mm, the maximum sample thickness thinning for EMF was 4.7% and 6.4% for conventional stamping, respectively. In the study carried out by Cai et al. [11], the EMF process and the deformation behavior of curved plates were analyzed by experimental and numerical methods. The experimental results showed that the initial profile of the workpiece could not achieve good flanging accuracy. The created numerical model was used to simulate the deformation process taking into account the electromagnetic force, the speed and the impact process, the size and distribution of the strains, and allowed the deformation behavior of the workpiece to be determined. Cui et al. [12] studied EMF with partitioning to obtain large curved parts that could be used in aircraft skins. Compared to conventional forming methods, EMF can significantly reduce springback when making curved parts for aircraft skins. In addition, numerical simulation was used to analyze the plate deformation, springback, stress and strain distribution. Commercial 5052 aluminum sheets punched with circular holes were studied for EMF and numerical simulation by Satonkar and Gopalan [13]. The results of the finite element simulation with Ansys 22 software were compared with the strains calculated by a regression equation and gave an error of less than 10%, which proves the accuracy of the regression model. The paper by Zhou et al. [14] presents a multiphysics computational framework for efficient finite element simulation of the EMF processes. The authors propose a reduction coefficient k that takes into account the variation of the magnetic field intensity, both with time (explicit) and with spatial distance (implicit). Incorporation of the reduction coefficient k allows one-way coupling of the electromagnetic

and mechanical domains. This 3D numerical analysis is more accurate and efficient for large domains and complex geometries compared to electromagnetic-mechanical analysis performed with fully coupled models.

The problem of EMF coils is addressed by Cao et al. [15], being known that lifetime of them is limited due to the high mechanical and thermal loads to which they are subjected. To solve this problem, the authors propose an electromagnetic coil-less sheet forming system, which additionally provides a uniform deformation pressure, and numerically model the system with a coupled electromagnetic-mechanical 3D model. Aspects regarding the deformation behavior, formability and microstructure of heat-treated and EMF Al-Li alloys are also addressed by Xie et al. [16,17]. The 2195 Al-Li alloy has low formability at room temperature, which is why the authors proposed a fabrication process that includes solution treatment, EMF and aging. The results show that the yield strength and tensile strength of the Al-Li alloy are 61% and 96% higher than those in the annealed state, with a better hardening rate. The EMF elongation after fracture for the Al-Li alloy is 35%, which is 52% higher than that at quasi-static stress. The microstructure evolution of the Al-Li alloy during the process was investigated by means of microscopic characterization. The proposed process achieves higher strain hardening and precipitation hardening with considerable plasticity and fracture toughness of Al-Li alloys. The process of heat treatment and EMF is also addressed by Xiao et al. [18] for the processing of 2024 aluminum alloy. Three thermal and EMF treatment schemes were proposed by the authors and the results obtained showed samples that presented the highest strength, as well as samples that had the highest elongation and corrosion resistance depending on the treatment variant applied. Research by Liu et al. [19] set out to investigate the strain uniformity at multiple two-coil EMF. By controlling the deformation energy and the movement of the coils, optimum conditions for the forming uniformity of large aluminum alloy metal sheet parts were obtained by applying multiple EMF. For fracture prediction of 6061 aluminum alloy subjected to EMF, Doley et al. [20] performed free bulging experiments and numerical simulations. The experimental results confirm the finite element simulations and establish the cause that produces the rupture of the material.

Xiao et al. [21] propose a new method of forming materials with low formability, namely electrically assisted EMF. Application of the new method to the forming of 7075 aluminum alloy showed an increase in strains of more than 40% compared to EMF and about 80% compared to quasi-static deformation. At the same time, they decreased the yield strength by 3.6%, the tensile strength by 2.6%, while the elongation increased by about 21% using electrically assisted EMF. Another new method of sheet forming is proposed by Zhao et al. [22], EMF combined with hydraulic forming called electromagnetic hydroforming. Free bulging dynamic deformation of 5052 aluminum alloy was analyzed during EMF and electromagnetic hydroforming processes. The EMF process resulted in a deformed part with an uneven conical shape, while electromagnetic hydroforming led to a deformed part with a regular circular shape, due to the uniform distribution of liquid pressure on the sheet surface. An electromagnetic hydraulic bulge experiment is proposed by Cheng et al. [23] to establish the strain-rate dependent hardening model for metal sheet subjected to EMF. Electromagnetic hydraulic bulging experiments were conducted on SUS304 stainless steel and 5052-O aluminum alloy sheet. The dynamic yield stress curves of stainless steel and aluminum alloy sheets were higher than those determined under quasi-static conditions. Electromagnetic hydraulic forming is also applied by Yan et al. [24] to study the deformation behavior of 5052 aluminum alloy sheets. The experimental study revealed that the parts obtained by electromagnetic hydraulic forming have a greater deformation depth compared to the parts made by hydraulic forming. Numerical simulation studies show that the deformation velocity exceeds 55 m/s and strain rate is close to 700 s^{-1} .

Reducing the springback after metal sheet forming remains a topical objective. Xia et al. [25] designed two forming processes that include EMF. The influence of different discharge voltages on the springback was analyzed in the two forming processes by finite element simulation, and the simulation results accurately predict the deformation

and springback of the sheet after quasi-static stamping and subsequent EMF. Cui et al. [26] studied, numerically and experimentally, the influence of the sheet thickness and the current damping exponent on the discharge current frequency and, implicitly, on the EMF result. An electromagnetic bulging process of the sheet was approached, the 2D simulation method providing results that are in agreement with the experimental results. Numerical studies about the influence of the discharge current frequency on the EMF results are also presented in paper [27]. The author noted that the increase in the discharge current frequency has a complex action on the maximum deformation pressure, meaning that a continuous decrease in the radial component of the pressure can be observed, while the axial component presents an increase that reaches a maximum for a certain value of the frequency. The discharge current frequency's effect on the components of the deformation pressure can be favorably exploited according to the aims followed in various applications, when the displacement of the workpiece's material is necessarily made mainly in radial or axial directions. The formability of aluminum alloy sheet in an EMF hemming process is studied by Shang et al. [28]. The authors present the experimental results of 6061-T6 aluminum sheets EMF hemming and discuss the effects of this process on the hem quality. Numerical simulation results of electromagnetic hemming are presented to facilitate a better understanding of the process.

In EMF processes, the rise in working coil temperature as a result of Joule heating can affect coil durability and efficiency. Du et al. [29] have proposed a simple method to solve this problem, which consists in fitting an additional resistor in the discharge circuit. With a 400 mΩ resistor, over 50% reduction in Joule heating in the coil was achieved. The effectiveness of the method was proven by numerical simulations and verified by experimental tests. Lin et al. [30] investigated the effects of die counter-impact on aluminum alloy sheet during EMF. The Gurson-Tvergaard-Needleman damage model was used for the numerical simulations of free and die EMF. After various EMF experiments, the aluminum alloy parts were studied with the optical microscope and the Vickers hardness was measured. In the paper [31], Zhang et al. studied the deformation behavior of circular hole-flanging obtained by EMF and stamping. Numerical simulations were performed to analyze the deformation of the 5052 aluminum alloy sheet and the stress-strain characteristics obtained by the two forming processes. The simulation results agree with the experimental ones. Yu et al. [32] investigated the EMF use to perform flanging of elongated holes. The research reveals a low accuracy of the geometry around the elongated hole flange and unequal flange heights, but the results obtained and the method proposed in the paper present important recommendations for the EMF flanging process of elongated holes or other irregular holes. The deformation behavior of 2524-T3 aluminum alloy sheet was investigated by Fang et al. [33] in a multi-step EMF process. The authors experimentally analyze the effects of process configurations, incremental range, discharge voltage, as well as sheet thickness on bend radius and strain height, and provide useful conclusions for future applications. Multi-point die electromagnetic incremental forming is applied to large parts with various curved shapes by combining electromagnetic incremental forming with multi-point die [34]. A finite element model has been established and, during the first discharge of the coil, the deformation process of large sheets is discussed. The simulation results are practically consistent with the experimental ones. The feasibility of this technology is verified by the electromagnetic incremental training experiment at several points.

The grain refinement mechanism and texture evolution of electromagnetically formed polycrystalline Cu sheets were investigated by Gao et al. [35]. They used the electron back-scattered diffraction technique and found that the average grain size decreased from 35.88 μm to 8.77 μm. The grain refinement was explained by the dynamic recrystallization occurring in the grain boundary regions of the samples, and an inhomogeneous dislocation density plus a large misorientation of the crystal lattice were closely observed.

As a conclusion of the presented studies, at the moment there are researchers' concerns for expanding the range of materials that can be processed by EMF. Most studies are made on aluminum alloys, but more and more researches appear in relation to the forming

of titanium. There is also interest for steel or copper processed by EMF. Concerns are also noted for applying EMF to large parts with various curves and holes. The EMF method is developed by introducing incremental forming, heat treatment or heating and combining it with the hydraulic forming method. In this paper, the free bulging process by EMF was proposed to study the deformation behavior and strains of three materials. The experimental investigations were carried out with sheets from AlMn0.5Mg0.5 (EN AW-3105), Cu-OF and FeP04 (deep drawing steel), which were formed in a specific range of deformation energies established for each material. The strains of the parts obtained by EMF were determined by the mesh method. The experimental data was processed by statistical methods, then the regression equations were obtained by which the strains of the parts from the tested materials can be calculated.

2. Materials and Methods

In order to perform the experimental program, three categories of metallic materials in rolled sheet form were used: aluminum alloy AlMn0.5Mg0.5 (paramagnetic), copper Cu-OF (diamagnetic) and steel FeP04 (ferromagnetic). The chemical composition of the three metallic materials is presented in Tables 1–3 (according to the manufacturer’s specifications).

Table 1. Composition (wt%) of AlMn0.5Mg0.5 aluminum alloy (sheet with 0.43 mm thickness).

Si	Fe	Cu	Mn	Mg	Cr	Zn	Ti	(Ni)	Al
0.27	0.33	0.11	0.46	0.72	0.069	0.03	0.019	0.05	Balance

Table 2. Composition (wt%) of Cu-OF material (sheet with 0.5 mm thickness).

Cu	Bi	Cd	P	Hg	O ₂	Pb	Se	S	Te	Zn
99.95	0.001	0.0001	0.0003	0.0001	0.001	0.001	0.001	0.0018	0.001	0.0001

Table 3. Composition (wt%) of FeP04 steel (sheet with 0.5 mm thickness).

C	P	S	Mn	Others (Si)	Others (Al)
0.08	0.014	0.012	0.40	0.06	0.025

The materials were subjected to tensile tests in order to determine the characteristic parameters. The tests were carried out at a temperature of 20 °C, and the samples used for were of the non-proportional type, where the gage length does not depend on the cross-sectional area and had a value of 80 mm. The samples for tensile tests were taken so that the stress axis formed angles of 0°, 45° and 90° with the rolling direction of the sheets from which they came. The results obtained regarding the elastic and plastic characteristics for the tested materials are indicated in Table 4. The notations in Table 4 represent: E is the elasticity modulus, $R_{p\ 0.2}$ is the conventional yield strength, R_m is the ultimate tensile strength and A_{80} is the percentage elongation at fracture.

From these materials, 110 mm disk specimens were prepared and printed with a mesh on one side. The mesh pitch in the radial direction was 5 mm and the angular pitch was 15°. These were then freely deformed on a die of 80 mm diameter and 5 mm draw radius, each with a different value of applied energy E , keeping the capacitance C of the capacitors constant at the value of 200 μF and changing its charging voltage V (Figure 1).

The charging voltage of the capacitor bank is adjustable between 1 and 10 kV. The total capacitance of the capacitor bank is provided by 4 capacitors of 50 μF, specially constructed for impulse discharge. The electromagnetic bulging tests were carried out with a device equipped with a blank-holder in two working variants, namely: with and without clamping of the specimen edge movement. The disks were deformed with a 5 turns spiral coil made of high-purity copper with the gap between the coil and the specimen of 1 mm. Some of the parts obtained are shown in Figure 2.

Table 4. Characteristics values determined by tensile tests.

Material/Sample Code	E [MPa]	$R_{p0.2}$ [MPa]	R_m [MPa]	A_{80} , %
AlMn0.5Mg0.5/0°	78,764	158.1	173.7	3.05
AlMn0.5Mg0.5/45°	78,518	152.6	169.4	4.95
AlMn0.5Mg0.5/90°	82,198	165.7	182.1	3.85
Average	79,827	158.8	175.1	3.95
Cu-OF/0°	119,710	298.3	307.7	1.72
Cu-OF/45°	112,530	284.3	288.8	4.30
Cu-OF/90°	133,837	297.4	301.4	1.56
Average	122,026	293.3	299.3	2.53
FeP04/0°	191,188	224.0	324.0	32.71
FeP04/45°	205,143	245.2	336.8	28.63
FeP04/90°	219,099	258.0	339.1	32.76
Average	205,143	242.4	333.3	31.37

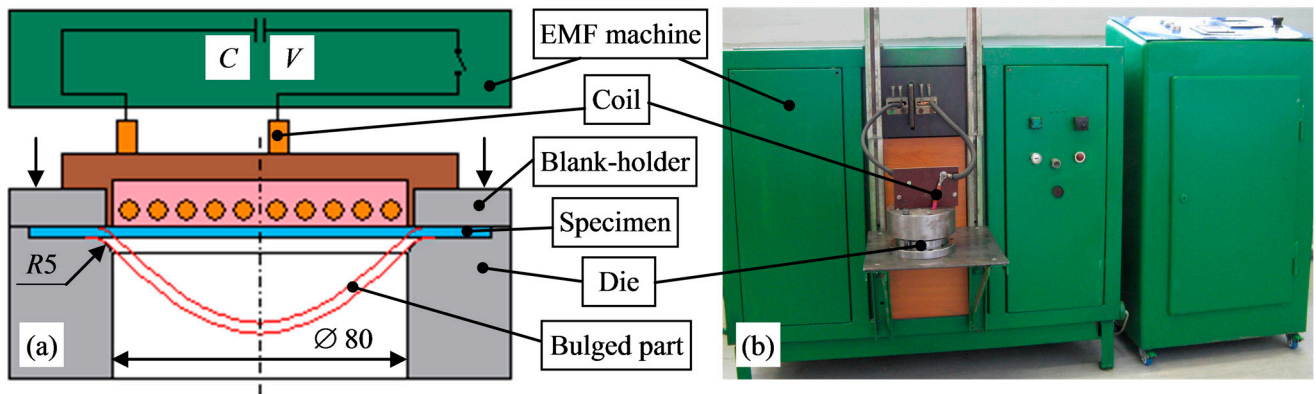


Figure 1. Experimental setup: (a) EMF schematic diagram; (b) EMF machine view.

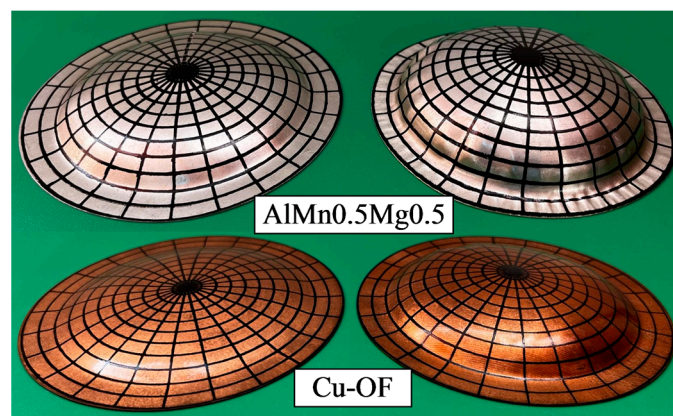


Figure 2. Parts with mesh obtained by EMF used for strains study.

The measurement of the axial displacements dz was carried out by placing the deformed part on a control table, on which a magnetic support was fixed and a dial comparator was attached, positioned in the center of the part. By moving the part in the radial direction r , the axial displacement of the part’s material was measured in each mesh node with a precision of ± 0.01 mm. The measurement of radial displacements dr (and tangential) was carried out with the help of a microscope for measuring lengths and angles with an accuracy of ± 0.001 mm. The scheme for measuring and calculating the radial displacements is

shown in Figure 3. As it can be seen from the figure, the deformed part is fixed on the table of the universal microscope and moves with it by means of micrometric mechanisms until the center of the part is brought to the reading axis of the microscope. Next is the reading of displacement value recorded in the respective direction which will constitute the origin of the dimensions chain that will be measured.

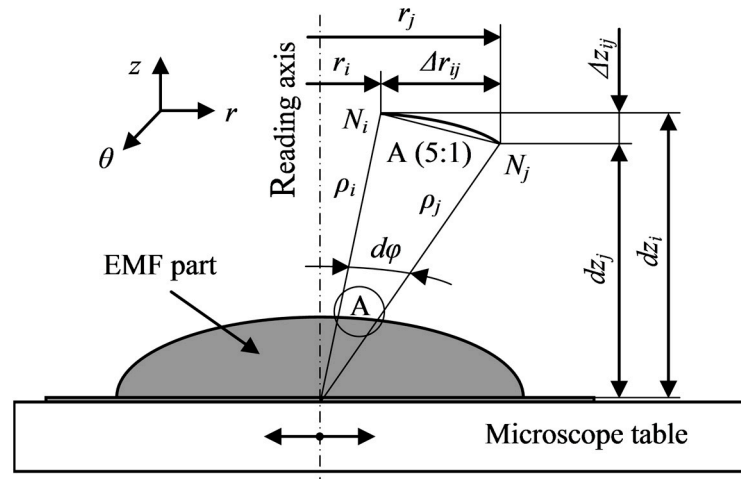


Figure 3. Measuring scheme of radial displacements.

After this, by moving the part in the radial direction r , the mesh nodes will be successively brought to the reading axis N_i, N_j, \dots , for which the values of the corresponding radial displacements are noted, the values of the axial displacements being previously determined. By moving the microscope table on the second coordinate, readings can be made to calculate the displacement of the nodes in the tangential direction θ .

Knowing the axial dz and radial dr displacements of the part's material in each mesh node, the radial strains calculation is done with the general relationship:

$$\epsilon_r = \frac{le_1 - le_0}{le_0} \times 100\% \tag{1}$$

where le_0 is the initial length of the mesh element, and the final length of the mesh element is calculated for each individual element based on the formula,

$$le_{1(ij)} = \text{arc length } N_i N_j \approx \overline{N_i N_j} = \sqrt{\Delta r_{ij}^2 + \Delta z_{ij}^2} \tag{2}$$

The arc length $N_i N_j$ is approximated by the chord length $\overline{N_i N_j}$, because the error introduced by this approximation is small, considering that the radial pitch (distance between two nodes) of the mesh on the workpieces is small.

The calculation of tangential strains is done with the help of the general relationship:

$$\epsilon_\theta = \frac{larc_1 - larc_0}{larc_0} \times 100\% \tag{3}$$

where the initial length of the arc element is $larc_{0(i)} = \frac{\pi}{180} r_{0(i)} \theta$, with $r_{0(i)}$ initial radius of the node N_i and the center angle $\theta = 15^\circ$, and the final length of the arc element is calculated for each individual element based on the formula,

$$larc_{1(i)} = \frac{\pi}{180} r_{1(i)} \theta \tag{4}$$

where $r_{1(i)}$ is the final radius of the node N_i .

The thinning measurement of the part's material is necessary for the calculation of the axial strains (in thickness), which is carried out based on the relationship:

$$\varepsilon_{z(t)} \equiv \varepsilon_z = \frac{t_1 - t_0}{t_0} \times 100\% \quad (5)$$

where t_0 is the initial thickness of the workpiece and t_1 is the final thickness of the formed part.

To measure the thinning of the material, the deformed part is placed on supports on a table with column device, on which a dial comparator is fixed. Coaxial with the comparator rod and on the opposite side, a fixed rod with a ball tip from another comparator is mounted at the upper end. By moving the part in the radial direction r , the final thickness of the part material is measured in each node of the mesh. The accuracy of measuring the final thicknesses based on the proposed scheme is ± 0.01 mm.

The chosen method for processing experimental data and establishing mathematical models is the regression analysis. First, the data obtained from the experimental program are subjected to processing through dispersion and correlation analyzes for the selection of factors with significant influence, the required number of tests establishment, the intensity of interaction between the factors assessment, the linearity or non-linearity of the links between the process parameters assessment. Then follows the actual mathematical model development with the help of regression analysis and statistical analysis of the established model, which assesses the compatibility between the established model and the real process.

The regression analysis sought to determine some mathematical models that reproduce the variation of axial and radial deformation degrees, in the plane-meridian section, for all the materials tested and all the energies applied. For data modeling containing two variables, it is recommended to use polynomial functions and apply linear regression analysis, or non-linear as the case may be, of an independent variable. The regression solution consists in the establishment of the mathematical model coefficients, which can be easily done with the help of the computer if the approximation polynomial is written in this form:

$$y = b_0P_0(x) + b_1P_1(x) + \dots + b_nP_n(x) \quad (6)$$

where $b_0, b_1 \dots b_n$ are the polynomial coefficients and $P_0(x), P_1(x) \dots P_n(x)$ are the orthogonal polynomials on the set of points $x_0, x_1 \dots x_n$.

3. Results and Discussion

Following the measuring procedure presented in Section 2, the axial displacements of the mesh nodes were obtained and served for determining the shape (profile) of electromagnetically formed parts (Figure 4). The profile of the electromagnetically formed parts highlights that the shape of the parts obtained from the three tested materials is different. Thus, aluminum alloy and copper parts show a tendency for maximum deformation in the center, while steel parts show a more uniform deformation over the entire surface. When restraining is applied with edge clamping of the workpieces, a tendency is observed for the shape of the electromagnetically formed parts to become conical. By means of data found from the measurements of axial and radial displacements, as well as from material thinning, axial and radial strains were calculated.

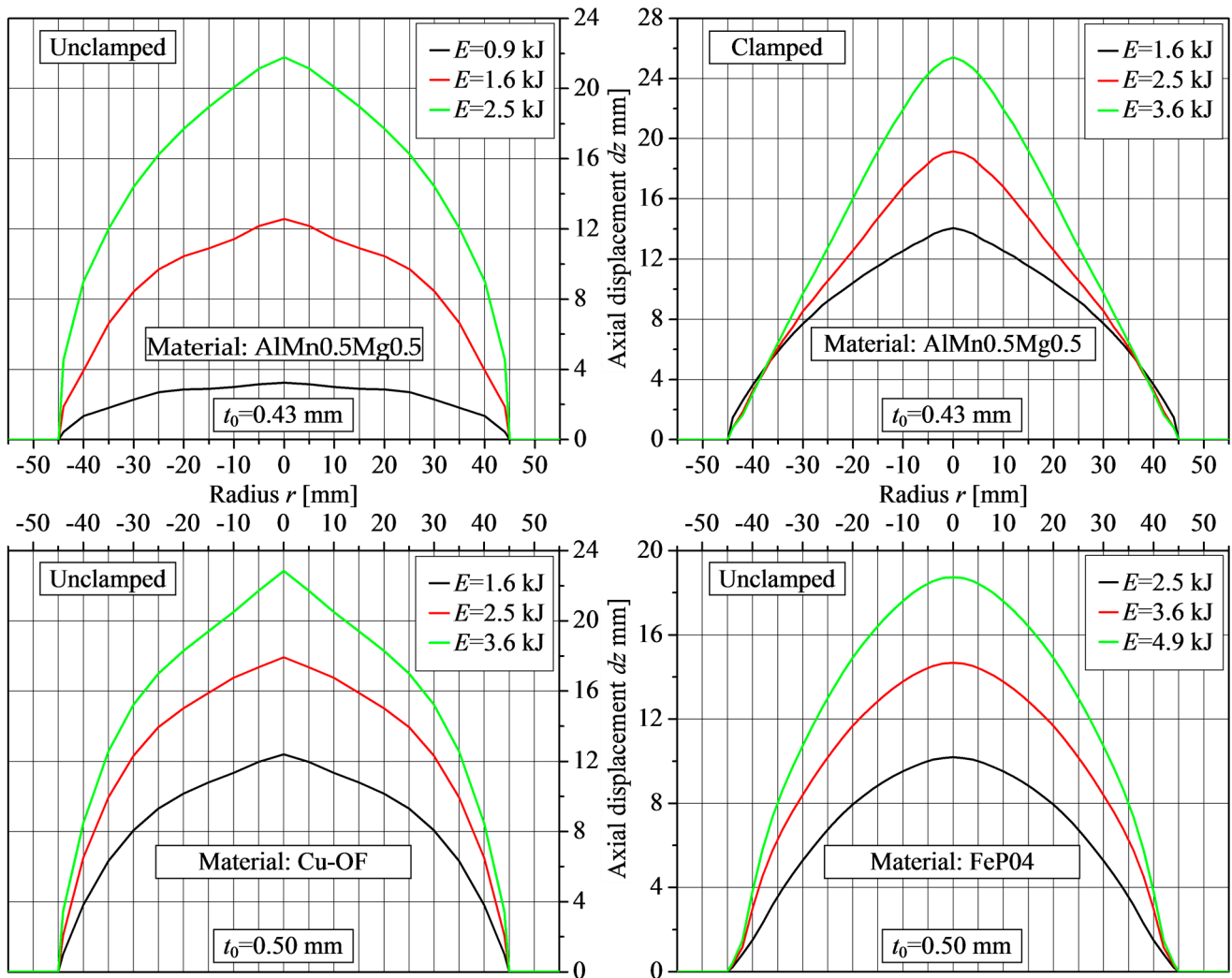


Figure 4. Profile of EMF parts made from the materials used in research.

The data obtained in this way for axial strains was subjected to correlation analysis, the results of which are presented in Table 5.

In order to be able to express the connection between the variables $Y(\epsilon_z)$ and $X(r)$, the indicator called simple correlation coefficient was used, whose estimate r_{yx} is determined with the relationship:

$$r_{yx} = \frac{\sum_{i=1}^n x_i y_i - n \bar{x} \bar{y}}{(n-1) S_x S_y} \tag{7}$$

where S_x and S_y represent the estimated mean squared deviations and n is the number of determinations.

After calculating the correlation coefficients, their significance was checked. Thus, in the case of simple correlation coefficient the Student criterion is used, which is expressed by the relationship:

$$t_c = \frac{|r_{yx}| \sqrt{v}}{\sqrt{1 - r_{yx}^2}} \tag{8}$$

where $v = n - 2$ represents the number of freedom degrees and n is the number of determinations.

The calculated values of the Student criterion (t_c) were compared with its tabled values (t_i), values that are chosen based on the level of significance ($\alpha = 0.05$) and the number

of freedom degrees ($\nu = 10$). It is considered that there is a correlation between the two variables if $t_c > t_t$.

By processing the experimental data listed in Table 5, for material thinning ($\epsilon_{z(t)} \equiv \epsilon_z$) in the cross-section of electromagnetically formed parts, mathematic models were obtained. According to the experimental data above, they had to be fitted with the polynomial function of order 6. Origin 9.9 software was used to do the regression analysis of the experimental data.

Table 5. Results of simple correlation analysis for strains ϵ_z .

Material	AlMn0.5Mg0.5			AlMn0.5Mg0.5 (*)			Cu-OF			FeP04			
E [kJ]	0.9	1.6	2.5	1.6	2.5	3.6	1.6	2.5	3.6	2.5	3.6	4.9	
x (r) [mm]	y (ϵ_z) %			y (ϵ_z) %			y (ϵ_z) %			y (ϵ_z) %			
0	-4.7	-9.3	-13.9	-13.9	-20.9	-25.6	-6.0	-9.0	-14.0	-11.0	-12.0	-14.0	
5	-4.7	-9.3	-12.8	-17.4	-24.4	-29.1	-5.0	-8.0	-12.0	-11.0	-12.0	-14.0	
10	-3.5	-8.1	-10.5	-15.1	-23.2	-27.9	-4.0	-7.0	-9.0	-12.0	-13.0	-15.0	
15	-2.9	-7.0	-9.3	-9.3	-16.3	-20.9	-3.0	-6.0	-7.0	-12.0	-14.0	-15.0	
20	-2.3	-4.7	-9.3	-8.1	-11.6	-15.1	-3.0	-4.0	-6.0	-11.0	-14.0	-16.0	
25	-2.3	-3.5	-5.8	-7.0	-11.6	-18.6	-2.0	-3.0	-4.0	-11.0	-13.0	-15.0	
30	-1.7	-2.3	-4.7	-5.8	-10.5	-16.3	-1.5	-2.0	-3.0	-9.0	-12.0	-13.0	
35	-1.2	-2.3	-3.5	-5.8	-10.5	-15.1	-1.0	-1.5	-2.0	-9.0	-11.0	-12.0	
40	-0.6	-1.2	-2.3	-4.6	-9.3	-11.6	-0.5	-0.5	-1.5	-8.0	-10.0	-11.0	
45	0	-0.6	-1.2	-2.3	-7.0	-9.3	0	0	-0.5	-3.0	-4.0	-6.0	
50	0	0	0	0	0	0	0	0	0	0	-2.0	-1.0	
55	0	0	0	0	0	0	0	0	0	0	0	0	
Correlation coefficient, r_{yx}	0.983	0.975	0.989	0.957	0.951	0.949	0.972	0.971	0.962	0.871	0.813	0.832	
Student criterion	t_c	16.744	13.867	21.018	10.391	9.704	9.499	13.152	12.939	11.183	5.605	4.420	4.743
	t_t	$t_{(0.05;10)} = t_t = 2.228$											
Verification	$t_c > t_t$	$t_c > t_t$	$t_c > t_t$	$t_c > t_t$	$t_c > t_t$	$t_c > t_t$	$t_c > t_t$	$t_c > t_t$	$t_c > t_t$	$t_c > t_t$	$t_c > t_t$	$t_c > t_t$	$t_c > t_t$
Validation	The correlation exists			The correlation exists			The correlation exists			The correlation exists			

(*) Experiment carried out with clamping the movement of the workpiece edge.

For the material AlMn0.5Mg0.5 without edge clamping ($E = 0.9; 1.6$ and 2.5 kJ):

$$\epsilon_z = -4.661 - 0.242r + 0.074r^2 - 0.005r^3 + 1.764 \times 10^{-4}r^4 - 2.673 \times 10^{-6}r^5 + 1.520 \times 10^{-8}r^6 \tag{9}$$

$$\epsilon_z = -9.295 - 0.003r + 0.018r^2 + 7.5 \times 10^{-4}r^3 - 6.943 \times 10^{-5}r^4 + 1.532 \times 10^{-6}r^5 - 1.089 \times 10^{-8}r^6 \tag{10}$$

$$\epsilon_z = -14.066 + 0.481r - 0.037r^2 + 0.003r^3 - 8.635 \times 10^{-5}r^4 + 1.307 \times 10^{-6}r^5 - 7.600 \times 10^{-9}r^6 \tag{11}$$

For the material AlMn0.5Mg0.5 with edge clamping ($E = 1.6; 2.5$ and 3.6 kJ):

$$\epsilon_z = -13.938 - 2.040r + 0.342r^2 - 0.018r^3 + 4.457 \times 10^{-4}r^4 - 4.979 \times 10^{-6}r^5 + 2.027 \times 10^{-8}r^6 \tag{12}$$

$$\epsilon_z = -20.837 - 1.845r + 0.236r^2 - 0.006r^3 - 6.642 \times 10^{-5}r^4 + 4.293 \times 10^{-6}r^5 - 4.003 \times 10^{-8}r^6 \tag{13}$$

$$\epsilon_z = -25.421 - 2.308r + 0.354r^2 - 0.016r^3 + 2.638 \times 10^{-4}r^4 - 7.536 \times 10^{-7}r^5 - 1.165 \times 10^{-8}r^6 \tag{14}$$

For the material Cu-OF without edge clamping ($E = 1.6; 2.5$ and 3.6 kJ):

$$\epsilon_z = -6.011 + 0.181r + 0.011r^2 - 0.001r^3 + 4.950 \times 10^{-5}r^4 - 8.283 \times 10^{-7}r^5 + 5.011 \times 10^{-9}r^6 \tag{15}$$

$$\varepsilon_z = -8.972 + 0.180r - 0.004r^2 + 0.001r^3 - 4.707 \times 10^{-5}r^4 + 8.489 \times 10^{-7}r^5 - 5.447 \times 10^{-9}r^6 \quad (16)$$

$$\varepsilon_z = -14.058 + 0.383r + 0.024r^2 - 0.002r^3 + 5.833 \times 10^{-5}r^4 - 7.828 \times 10^{-7}r^5 + 3.921 \times 10^{-9}r^6 \quad (17)$$

For the material FeP04 without edge clamping ($E = 2.5; 3.6$ and 4.9 kJ):

$$\varepsilon_z = -11.004 + 0.436r - 0.137r^2 + 0.012r^3 - 4.756 \times 10^{-4}r^4 + 8.356 \times 10^{-6}r^5 - 5.447 \times 10^{-8}r^6 \quad (18)$$

$$\varepsilon_z = -12.008 + 0.432r - 0.124r^2 + 0.010r^3 - 3.470 \times 10^{-4}r^4 + 5.825 \times 10^{-6}r^5 - 3.704 \times 10^{-8}r^6 \quad (19)$$

$$\varepsilon_z = -14.087 + 0.643r - 0.170r^2 + 0.014r^3 - 4.946 \times 10^{-4}r^4 + 8.361 \times 10^{-6}r^5 - 5.316 \times 10^{-8}r^6 \quad (20)$$

Figure 5 shows the variation of axial strains in a plane-meridian section.

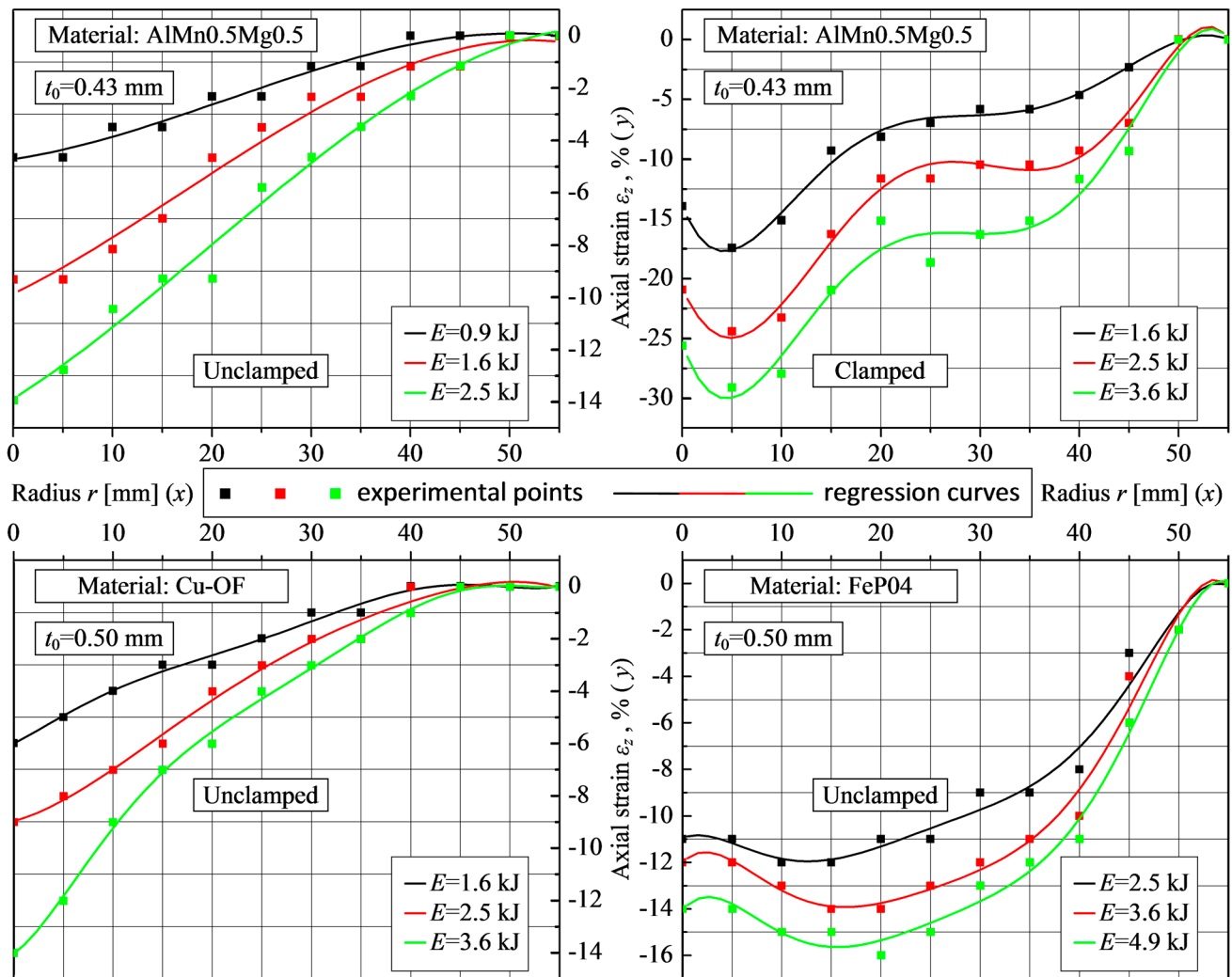


Figure 5. Thinning variation of the EMF parts from the materials used for experiments.

After determining the mathematical models, their verification and statistical validation were accomplished. The determined models were verified using the Fischer criterion, given by the relationship:

$$F_c = \frac{S_{md}^2}{S_{rr}^2} \quad (21)$$

where S_{md}^2 is the dispersion of the determined model and S_{rr}^2 is the reproducibility dispersion of the results.

The calculated values of the Fischer criterion (F_c) were compared with its tabled values (F_t). The tabled values are chosen based on the level of significance ($\alpha = 0.05$), the

number of freedom degrees with which it is calculated S_{md}^2 ($\nu_1 = n - p$), and the number of freedom degrees with which the dispersion S_{rr}^2 ($\nu_2 = r - 1$) is calculated. The term $n - p$ represents the difference between the number of determinations n and the number of coefficients p (including the free term) from the determined regression equation. The term r represents the number of repeated determinations ($r = 3$) in the center of the experiments (determination 5). It is considered that the determined mathematical model is adequate if the condition $F_c < F_t$ is verified.

Verification of the determined models for FeP04 material is summarized in Table 6.

Table 6. Results of regression analysis for the models (18), (19) and (20).

No. Determination (n)	FeP04								
	E = 2.5 kJ			E = 3.6 kJ			E = 4.9 kJ		
	y_{regr} %	y_{exp} %	Error %	y_{regr} %	y_{exp} %	Error %	y_{regr} %	y_{exp} %	Error %
1	-11.004	-11.0	0.039	-12.008	-12.0	0.067	-14.087	-14.0	0.621
2	-10.985	-11.0	-0.132	-11.921	-12.0	-0.658	-13.694	-14.0	-2.235
3	-12.031	-12.0	0.258	-13.208	-13.0	1.579	-15.111	-15.0	0.735
4	-12.022	-12.0	0.182	-13.901	-14.0	-0.712	-15.706	-15.0	4.493
5	-11.217	-11.0	1.936	-13.770	-14.0	-1.666	-15.288	-16.0	-4.656
6	-10.346	-11.0	-6.325	-13.185	-13.0	1.402	-14.472	-15.0	-3.647
7	-9.769	-9.0	7.877	-12.383	-12.0	3.095	-13.632	-13.0	4.638
8	-9.078	-9.0	0.859	-11.166	-11.0	1.486	-12.459	-12.0	3.688
9	-7.323	-8.0	-9.237	-9.003	-10.0	-11.075	-10.116	-11.0	-8.742
10	-3.871	-3.0	22.496	-5.557	-4.0	28.018	-5.985	-6.0	-0.248
11	0.141	0 (*)	- (*)	-1.625	-2.0	-23.068	-1.024	-1.0	2.389
12	-0.276	0	-	-0.496	0	-	0.289	0	-
Error	$S_{rr}^2 = 0.333$			$S_{rr}^2 = 0.333$			$S_{rr}^2 = 0.333$		
Model dispersion	$S_{md}^2 = 0.477$			$S_{md}^2 = 0.825$			$S_{md}^2 = 0.575$		
Fischer criterion	$F_c = 1.432$			$F_c = 2.475$			$F_c = 1.724$		
	$F_{(0.05,5;2)} = F_t = 19.30$								
Verification	$F_c < F_t$	True		$F_c < F_t$	True		$F_c < F_t$	True	
Validation	The model is adequate			The model is adequate			The model is adequate		

(*) For determinations where $y_{exp} = 0$ (due to measurement error) the modeling error calculation does not make physical sense.

The thinning of aluminum alloy and copper parts is at its maximum in the center and it decreases towards the outside, while the thinning of steel parts is smaller in the center and it reaches its maximum in an annular area roughly defined from $r = 10 \dots 25$ mm and decreases to the outside. Parts from AlMn0.5Mg0.5 deformed with edge clamping show a similar evolution to that of parts from FeP04. Models (9) ... (20) were established on statistical-mathematical bases for the thinning calculation of flat workpieces processed by EMF. The final part thicknesses show that processing by EMF of flat workpiece is accompanied by material thinning regardless of whether the deformation is done with or without clamping the workpiece edge movement.

Following the procedure applied to the study of the axial strains, the radial strains were established. Table 7 shows the results of the correlation analysis for these strains. The material elongation (ϵ_r) of electromagnetically formed parts can be determined based on the mathematical models below, determined by applying regression analysis to the data in Table 7.

Table 7. Results of simple correlation analysis for strains ϵ_r .

Material	AlMn0.5Mg0.5			AlMn0.5Mg0.5 (*)			Cu-OF			FeP04			
E [kJ]	0.9	1.6	2.5	1.6	2.5	3.6	1.6	2.5	3.6	2.5	3.6	4.9	
x (r) [mm]	y (ϵ_r) %			y (ϵ_r) %			y (ϵ_r) %			y (ϵ_r) %			
0	2.328	4.652	6.976	6.976	10.470	12.790	3.022	4.520	7.020	5.450	6.070	7.004	
5	2.126	4.250	6.396	8.722	12.210	14.530	2.478	3.780	5.380	5.542	6.320	7.052	
10	1.784	4.070	5.232	7.558	11.630	13.950	2.030	3.122	4.322	6.048	6.850	7.450	
15	1.702	3.488	4.852	4.652	8.138	11.270	1.470	2.798	3.496	6.500	7.300	7.518	
20	1.182	2.926	4.650	4.070	7.018	8.358	1.520	2.022	3.222	5.904	7.102	8.002	
25	1.146	2.144	2.908	3.488	6.014	8.702	0.980	1.478	1.998	5.650	6.650	7.446	
30	0.582	1.562	2.326	2.908	5.832	8.140	0.582	1.020	1.502	5.046	6.134	6.452	
35	0.380	1.162	1.744	2.706	5.224	7.558	0.424	0.700	0.980	4.410	4.550	6.080	
40	0.102	0.882	1.162	2.326	4.652	5.814	0.188	0.304	0.624	3.812	4.518	5.450	
45	0	0.524	0.584	1.162	3.788	4.952	0.072	0.116	0.356	2.152	2.422	3.040	
50	0	0	0	0	0	0	0	0	0.064	1.094	1.180	1.352	
55	0	0	0	0	0	0	0	0	0	0	0	0	
Correlation coefficient, r_{yx}	-0.977	-0.991	-0.989	-0.957	-0.959	-0.956	-0.966	-0.973	-0.963	-0.868	-0.851	-0.839	
Student criterion	t_c	14.434	23.267	21.163	10.479	10.705	10.264	11.750	13.349	11.322	5.521	5.121	4.868
	t_t	$t_{(0.05;10)} = t_t = 2.228$											
Verification	$t_c > t_t$	$t_c > t_t$	$t_c > t_t$	$t_c > t_t$	$t_c > t_t$	$t_c > t_t$	$t_c > t_t$	$t_c > t_t$	$t_c > t_t$	$t_c > t_t$	$t_c > t_t$	$t_c > t_t$	$t_c > t_t$
Validation	The correlation exists			The correlation exists			The correlation exists			The correlation exists			

(*) Experiment carried out with clamping the movement of the workpiece edge.

The analysis applied first was simple linear regression, which proved inadequate as in the case of axial strains, after which simple non-linear regressions using polynomials of increasing degree were successively applied until the maximum correlation between calculated and experimental data was achieved. According to the experimental results obtained for the strains ϵ_r , they had to be fitted with the polynomial function of order 6.

For the material AlMn0.5Mg0.5 without edge clamping ($E = 0.9; 1.6$ and 2.5 kJ):

$$\epsilon_r = 2.332 - 0.037r - 0.003r^2 + 2.7 \times 10^{-4}r^3 - 1.241 \times 10^{-5}r^4 + 2.458 \times 10^{-7}r^5 - 1.693 \times 10^{-9}r^6 \tag{22}$$

$$\epsilon_r = 4.654 - 0.172r + 0.029r^2 - 0.003r^3 + 9.502 \times 10^{-5}r^4 - 1.546 \times 10^{-6}r^5 + 9.341 \times 10^{-9}r^6 \tag{23}$$

$$\epsilon_r = 7.034 - 0.275r + 0.028r^2 - 0.002r^3 + 6.749 \times 10^{-5}r^4 - 1.027 \times 10^{-6}r^5 + 5.962 \times 10^{-9}r^6 \tag{24}$$

For the material AlMn0.5Mg0.5 with edge clamping ($E = 1.6; 2.5$ and 3.6 kJ):

$$\epsilon_r = 6.972 + 1.012r - 0.170r^2 + 0.009r^3 - 2.231 \times 10^{-4}r^4 + 2.523 \times 10^{-6}r^5 - 1.050 \times 10^{-8}r^6 \tag{25}$$

$$\epsilon_r = 10.460 + 0.836r - 0.107r^2 + 0.003r^3 + 2.120 \times 10^{-5}r^4 - 1.736 \times 10^{-6}r^5 + 1.658 \times 10^{-8}r^6 \tag{26}$$

$$\epsilon_r = 12.750 + 0.848r - 0.101r^2 + 0.002r^3 + 6.079 \times 10^{-5}r^4 - 2.568 \times 10^{-6}r^5 + 2.270 \times 10^{-8}r^6 \tag{27}$$

For the material Cu-OF without edge clamping ($E = 1.6; 2.5$ and 3.6 kJ):

$$\epsilon_r = 3.030 - 0.125r + 0.002r^2 + 1.4 \times 10^{-4}r^3 - 9.874 \times 10^{-6}r^4 + 2.136 \times 10^{-7}r^5 - 1.523 \times 10^{-9}r^6 \tag{28}$$

$$\epsilon_r = 4.522 - 0.202r + 0.014r^2 - 9.0 \times 10^{-4}r^3 + 2.840 \times 10^{-5}r^4 - 4.107 \times 10^{-7}r^5 + 2.256 \times 10^{-9}r^6 \tag{29}$$

$$\epsilon_r = 7.038 - 0.496r + 0.039r^2 - 0.002r^3 + 6.013 \times 10^{-5}r^4 - 8.112 \times 10^{-7}r^5 + 4.236 \times 10^{-9}r^6 \tag{30}$$

For the material FeP04 without edge clamping ($E = 2.5; 3.6$ and 4.9 kJ):

$$\varepsilon_r = 5.443 - 0.136r + 0.048r^2 - 0.004r^3 + 1.357 \times 10^{-4}r^4 - 2.183 \times 10^{-6}r^5 + 1.327 \times 10^{-8}r^6 \quad (31)$$

$$\varepsilon_r = 6.083 - 0.113r + 0.045r^2 - 0.003r^3 + 1.134 \times 10^{-4}r^4 - 1.743 \times 10^{-6}r^5 + 1.030 \times 10^{-8}r^6 \quad (32)$$

$$\varepsilon_r = 7.032 - 0.206r + 0.056r^2 - 0.004r^3 + 1.510 \times 10^{-4}r^4 - 2.489 \times 10^{-6}r^5 + 1.555 \times 10^{-8}r^6 \quad (33)$$

Figure 6 shows the variation of radial strains in a plane-meridian section.

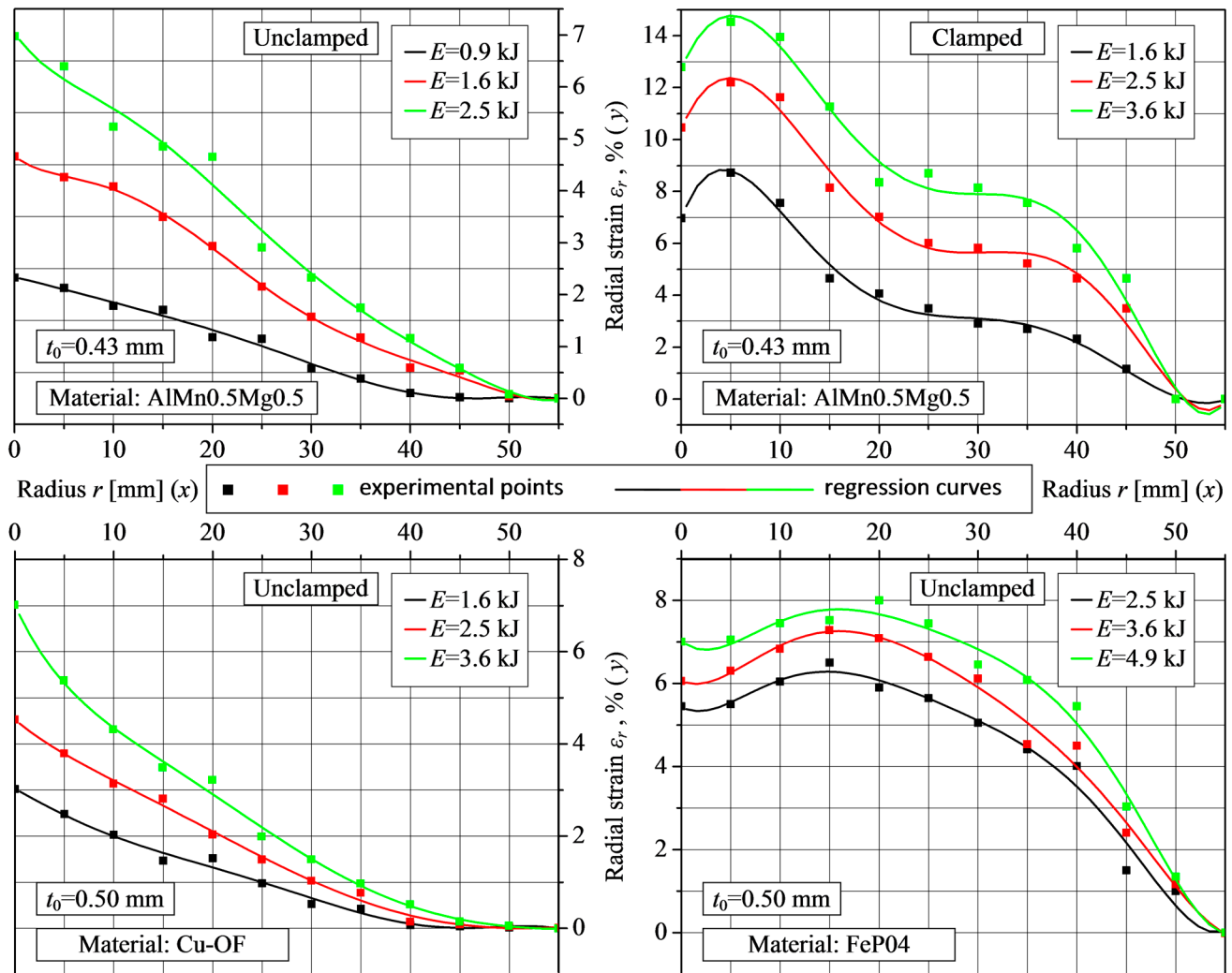


Figure 6. Elongation variation of EMF parts from the materials used for experiments.

The determination of the mathematical models was followed by their verification and statistical validation, the results of the checks for the radial strains being summarized in Table 8 for the AIMn0.5Mg0.5 material without edge clamping.

The elongation of the formed parts, for the three materials studied, varies according to the radius following the mathematical models (18) . . .(29). After the statistical verifications, it was proven that all the determined models are adequate. Although the parts were free-formed, it was found that the maximum elongation does not occur in the center for all materials (see Figure 6). Thus, meanwhile the copper parts present the maximum elongation in the center, for aluminum alloy and steel parts it is found that the central area has elongated less than the immediately nearby areas.

Table 8. Results of regression analysis for the models (22), (23) and (24).

No. Determination (n)	AlMn0.5Mg0.5 (Unclamped)								
	E = 0.9 kJ			E = 1.6 kJ			E = 2.5 kJ		
	y_{regr} %	y_{exp} %	Error %	y_{regr} %	y_{exp} %	Error %	y_{regr} %	y_{exp} %	Error %
1	2.332	2.328	0.169	4.654	4.652	0.044	7.034	6.976	0.827
2	2.102	2.126	-1.132	4.249	4.250	-0.014	6.134	6.396	-4.269
3	1.848	1.784	3.474	4.041	4.070	-0.711	5.585	5.232	6.313
4	1.594	1.702	-6.774	3.572	3.488	2.339	4.935	4.852	1.685
5	1.321	1.182	10.501	2.876	2.926	-1.755	4.123	4.650	-12.791
6	1.011	1.146	-13.392	2.165	2.144	0.955	3.253	2.908	10.607
7	0.673	0.582	13.564	1.615	1.562	3.257	2.451	2.326	5.107
8	0.352	0.380	-8.112	1.258	1.162	7.643	1.777	1.744	1.867
9	0.109	0.102	6.132	0.984	0.882	10.335	1.210	1.162	3.959
10	-0.003	0	-	0.638	0.524	17.875	0.698	0.584	16.295
11	0.009	0	-	0.235	0	-	0.276	0	-
12	0.003	0	-	0.270	0	-	0.252	0	-
Error	$S_{rr}^2 = 0.097$			$S_{rr}^2 = 0.456$			$S_{rr}^2 = 1.142$		
Model dispersion	$S_{md}^2 = 0.013$			$S_{md}^2 = 0.035$			$S_{md}^2 = 0.154$		
Fischer criterion	$F_c = 0.130$			$F_c = 0.076$			$F_c = 0.135$		
	$F_{(0.05;5;2)} = F_t = 19.30$								
Verification	$F_c < F_t$	True		$F_c < F_t$	True		$F_c < F_t$	True	
Validation	The model is adequate			The model is adequate			The model is adequate		

4. Conclusions

In this work, a study was made on the main strains that occur in metal sheet parts after EMF. The high-speed deformation behavior of three metallic materials (AlMn0.5Mg0.5, Cu-OF and FeP04) was studied by electromagnetic free bulging of 110 mm diameter metal sheet disks.

The main conclusions can be drawn as follows:

1. The shape (profile) of the electromagnetic free bulged parts is different, although the same coil and die were used in all tests for the three materials. This suggests that the magnetic properties and electrical conductivity of the three materials may have influences on the shape of the part obtained by EMF, which may be the subject of future studies;
2. Material forming in all three tested materials occurs through thickness thinning. Thus, although the same deformation tools were used for the three materials, the through thickness strains were maximum in the center of the AlMn0.5Mg0.5 and Cu-OF parts, while for the FeP04 parts (deep drawing steel) the thinning was lower in the center of them, maximum in an intermediate area, and decreased towards the edge;
3. The final thicknesses measured at the mesh nodes show that material thinning occurs when forming is done with the workpiece edge clamped, as expected, but thinning also occurs when the workpiece edge is allowed to move;
4. Material forming in all three tested materials also occurs through elongation. Radial strains have maximum values in the center of AlMn0.5Mg0.5 and Cu-OF parts and decrease towards the edge, while for FeP04 parts the evolution of elongation along the radius has a shape similar to the variation of thinning, with maximum values in an intermediate zone between the center and the edge;
5. The established mathematical models reproduce with high accuracy the variation of axial and radial strains along the radius of electromagnetically formed parts and are useful

tools for engineering calculations. By calculating the strains with the established regression equations, the areas where the strains reach maximum values and the danger of fracturing the material can be identified.

Author Contributions: Conceptualization, D.L.; methodology, D.L.; software, D.L. and D.D.L.; validation, D.L. and D.D.L.; investigation, D.L.; resources, D.L.; data curation, D.D.L.; writing—original draft preparation, D.L. and D.D.L.; writing—review and editing, D.L.; visualization, D.D.L.; supervision, D.L. All authors have read and agreed to the published version of the manuscript.

Funding: This research received no external funding.

Data Availability Statement: Not applicable.

Conflicts of Interest: The authors declare no conflict of interest.

References

1. Li, F.; Mo, J.; Li, J.; Zhao, J. Formability evaluation for low conductive sheet metal by novel specimen design in electromagnetic forming. *Int. J. Adv. Manuf. Technol.* **2017**, *88*, 1677–1685. [[CrossRef](#)]
2. Feng, F.; Li, J.; Huang, L.; Zhang, Y.; Cao, S.; Chen, R.; Fan, S. Thermoplastic forming of TC4 titanium alloy sheet by direct pulse current electromagnetic forming. *J. Mater. Sci.* **2022**, *57*, 14082–14095. [[CrossRef](#)]
3. Feng, F.; Li, J.; Huang, L.; Chen, R.; Fan, S. Direct pulse current electromagnetic forming (DPCEMF): A novel electromagnetic forming technology for aluminum alloy sheet. *Int. J. Adv. Manuf. Technol.* **2022**, *121*, 6059–6072. [[CrossRef](#)]
4. Cai, S. Pressure distributions generated by vaporizing metal foils. *Trans. Nonferrous Met. Soc. China* **2018**, *28*, 2062–2074. [[CrossRef](#)]
5. Dong, P.; Zhangzhe, L.; Sheng, F.; Zelin, W.; Quanliang, C.; Liang, L.; Qi, C.; Xiaotao, H. Fabrication of titanium bipolar plates for proton exchange membrane fuel cells by uniform pressure electromagnetic forming. *Int. J. Hydrogen Energy* **2021**, *46*, 38768–38781. [[CrossRef](#)]
6. Huang, L.; Wenjing, F.1; Jin, Z.1; Zinan, D. Research on the drive electromagnetic forming of aluminum alloy and parameter optimization. *Int. J. Adv. Manuf. Technol.* **2022**, *120*, 7101–7113. [[CrossRef](#)]
7. Liu, D.; Li, B.; Guo, Z.; Huang, Z. Finite element analysis on electromagnetic forming of DP780 high-strength steel sheets. *Int. J. Adv. Manuf. Technol.* **2021**, *112*, 1617–1629. [[CrossRef](#)]
8. Luca, D. Neural networks for parameters prediction of an electromagnetic forming process of FeP04 steel sheets. *Int. J. Adv. Manuf. Technol.* **2015**, *80*, 689–697. [[CrossRef](#)]
9. Jin, Y.; Yu, H. Enhanced formability and hardness of AA2195-T6 during electromagnetic forming. *J. Alloys Compd.* **2021**, *890*, 161891. [[CrossRef](#)]
10. Lin, Y.; Xiaohui, C.; Kanghua, C.; Ang, X.; Ziqin, Y. Forming limit and mechanical properties of 2024-O aluminum alloy under electromagnetic forming. *Met. Mater. Int.* **2022**, *28*, 2472–2482. [[CrossRef](#)]
11. Cai, D.; An, H.; Li, G.; Ou, H.; Cui, J.; Jiang, H. Local flanging process on a curved wind deflector using electromagnetic forming. *J. Manuf. Process.* **2022**, *84*, 1030–1041. [[CrossRef](#)]
12. Cui, X.; Du, Z.; Xiao, A.; Yan, Z.; Qiu, D.; Yu, H.; Chen, B. Electromagnetic partitioning forming and springback control in the fabrication of curved parts. *J. Mater. Process. Technol.* **2021**, *288*, 116889. [[CrossRef](#)]
13. Satonkar, N.; Gopalan, V. Simulation of electromagnetic forming process and optimization of geometric parameters of perforated Al sheet using RSM. *Mathematics* **2023**, *11*, 1983. [[CrossRef](#)]
14. Zhou, M.; Li, Z.; Assadi, H.; Chang, I.; Barbatti, C. An accelerated three-dimensional coupled electromagnetic-mechanical model for electromagnetic pulse forming. *J. Manuf. Process.* **2021**, *72*, 240–251. [[CrossRef](#)]
15. Cao, Q.; Li, X.; Li, Z.; Du, L.; Xia, L.; Lai, Z.; Chen, Q.; Han, X.; Li, L. Coil-less electromagnetic forming process with uniform-pressure characteristics for shaping sheet metals. *J. Manuf. Process.* **2021**, *70*, 140–151. [[CrossRef](#)]
16. Xie, B.; Huang, L.; Xu, J.; Wang, Y.; Xu, Y.; Zhang, H.; Li, J. Deformation behavior and formability of solid solution state Al-Li alloy in electromagnetic forming. *Mater. Sci. Eng. A* **2022**, *854*, 143858. [[CrossRef](#)]
17. Xie, B.; Huang, L.; Xu, J.; Wang, Y.; Li, J. Microstructure evolution and strengthening mechanism of Al-Li alloy during thermo-electromagnetic forming process. *J. Mater. Process. Technol.* **2023**, *315*, 117922. [[CrossRef](#)]
18. Xiao, A.; Yuhong, L.; Changqing, H.; Xiaohui, C.; Ziqin, Y.; Zhihao, D. Effect of electromagnetic forming-heat treatment process on mechanical and corrosion properties of 2024 aluminum alloy. *J. Mater. Res. Technol.* **2023**, *23*, 1027–1038. [[CrossRef](#)]
19. Liu, X.; Liang, H.; Jianjun, L.; Rongchuang, C.; Jinbo, L.; Chunwei, W.; Min, W.; Jingliang, L. Study on forming uniformity of multi-electromagnetic forming (EMF) of aluminum sheet metal. *Int. J. Adv. Manuf. Technol.* **2022**, *122*, 2671–2684. [[CrossRef](#)]
20. Doley, J.K.; Rajak, A.K.; Kumar, R.; Kore, S.D. Numerical and experimental validation for prediction of failure in electromagnetic forming of AA6061 sheet. *Trans. Indian. Inst. Met.* **2022**, *75*, 2977–2983. [[CrossRef](#)]
21. Xiao, A.; Changqing, H.; Ziqin, Y.; Xiaohui, C.; Shipeng, W. Improved forming capability of 7075 aluminum alloy using electrically assisted electromagnetic forming. *Mater. Charact.* **2022**, *183*, 111615. [[CrossRef](#)]
22. Zhao, P.; Ziqin, Y.; Xiaohui, C. Comparison of dynamic deformation using electromagnetic hydraulic forming and electromagnetic forming. *Int. J. Adv. Manuf. Technol.* **2022**, *119*, 8077–8089. [[CrossRef](#)]

23. Cheng, T.; Zhenghua, M.; Wei, L.; Jiaqi, L.; Jili, L.; Shangyu, H. Inverse identification of constitutive model for metallic thin sheet via electromagnetic hydraulic bulge experiment. *Int. J. Mater. Form.* **2023**, *16*, 38. [[CrossRef](#)]
24. Yan, Z.; Ang, X.; Peng, Z.; Xiaohui, C.; Hailiang, Y.; Yuhong, L. Deformation behavior of 5052 aluminum alloy sheets during electromagnetic hydraulic forming. *Int. J. Mach. Tool. Manuf.* **2022**, *179*, 103916. [[CrossRef](#)]
25. Xia, W.; Xiaohui, C.; Zhihao, D.; Zanshi, D.; Yuhong, L. Springback control with small vibration using electromagnetic forming. *Int. J. Adv. Manuf. Technol.* **2022**, *118*, 3133–3145. [[CrossRef](#)]
26. Cui, X.; Jianjun, L.; Jianhua, M.; Jinxiu, F.; Bo, Z.; Xiaoting, X. Effect of the sheet thickness and current damping exponent on the optimum current frequency in electromagnetic forming. *Int. J. Adv. Manuf. Technol.* **2016**, *85*, 843–851. [[CrossRef](#)]
27. Luca, D. A numerical modelling: Opened perspectives to increase the performance of the electromagnetic forming processes. *Int. J. Numer. Model. Electron. Netw. Dev. Fields* **2012**, *25*, 15–23. [[CrossRef](#)]
28. Shang, J.; Wilkerson, L.; Hatkevich, S. Hemming of aluminum alloy sheets using electromagnetic forming. *J. Mater. Eng. Perform.* **2011**, *20*, 1370–1377. [[CrossRef](#)]
29. Du, L.; Liangyu, X.; Xian, L.; Li, Q.; Zhipeng, L.; Qi, C.; Quanliang, C.; Xiaotao, H.; Liang, L. Adjustable current waveform via altering the damping coefficient: A new way to reduce Joule heating in electromagnetic forming coils. *J. Mater. Process. Technol.* **2021**, *293*, 117086. [[CrossRef](#)]
30. Lin, Y.; Wei, L.; Zhenghua, M.; Xiaoyong, Z.; Shangyu, H. The effects of die counter-impact on aluminum alloy sheet during electromagnetic forming. *Int. J. Adv. Manuf. Technol.* **2021**, *116*, 3593–3601. [[CrossRef](#)]
31. Zhang, L.; Xiaohui, C.; Qiang, D.; Ziqin, Y.; Shengping, Y. Comparison of the deformation behavior of circular hole-flanging obtained by electromagnetic forming and stamping. *Int. J. Adv. Manuf. Technol.* **2022**, *121*, 171–183. [[CrossRef](#)]
32. Yu, H.; Yanye, J.; Lan, H.; Huazhe, Y.; Sun, S. Two-step method to improve geometry accuracy of elongated hole flanging by electromagnetic forming. *Int. J. Adv. Manuf. Technol.* **2020**, *106*, 3117–3129. [[CrossRef](#)]
33. Fang, C.; Xiang, Z.; Li, L.; Wenping, W.; Min, W. Effects of process configuration and sheet thickness on the deformation behaviour in multi-step electromagnetic forming of aluminium alloy sheet. *Int. J. Adv. Manuf. Technol.* **2021**, *112*, 2565–2572. [[CrossRef](#)]
34. Feng, F.; Jianjun, L.; Rongchuang, C.; Liang, H.; Hongliang, S.; Suo, F. Multi-point die electromagnetic incremental forming for large-sized sheet metals. *J. Manuf. Process.* **2021**, *62*, 458–470. [[CrossRef](#)]
35. Gao, X.; Wu, J.; Zhao, J. Grain refinement mechanism and texture evolution of polycrystalline Cu sheets during the electromagnetic forming process. *J. Wuhan Univ. Technol. Mater. Sci. Ed.* **2019**, *34*, 1421–1428. [[CrossRef](#)]

Disclaimer/Publisher's Note: The statements, opinions and data contained in all publications are solely those of the individual author(s) and contributor(s) and not of MDPI and/or the editor(s). MDPI and/or the editor(s) disclaim responsibility for any injury to people or property resulting from any ideas, methods, instructions or products referred to in the content.